International Journal of Technology

http://ijtech.eng.ui.ac.id

Research Article

Validating CO Emission Reduction from B30 Diesel Engines through Exhaust-Heated Shell-and-Spiral Coil Fuel Preheating System

Parabelem Tinno Dolf Rompas[1*], Jenly Dyliep Isria Manongko[1], Jemmy Charles Kewas[1], Basyirun[2], Ahmad Tubagus Tsani Risqi Aji[3], Johni Jonatan Numberi[4], Éric Serre[5]

[1]Department of Mechanical Engineering, Universitas Negeri Manado, Tondano 95619, Indonesia

[2]Department of Doctoral Program Vocational Education, Universitas Negeri Semarang, Semarang 50232, Indonesia

[3]Department of Fishery Mechanization, Politeknik Kelautan dan Perikanan Bitung, Bitung 95526, Indonesia

[4]Department of Renewable Energy Engineering, Universitas Cenderawasih, Jayapura, Papua 99351, Indonesia

[5]Aix-Marseille Univ., Centre National de la Recherche Scientifique, Centrale Méd., M2P2, Marseille 13451, France

[*]Corresponding author: parabelemrompas@unima.ac.id; Tel.: +62-82292199519

Abstract: This fundamental research investigates the proof-of-concept effect of a counter-flow Shell-and-Spiral Coil Heat Exchanger (SSCHE) on CO emissions from a B30-fueled single-cylinder 7 HP diesel engine under no-load conditions, without dynamometer loading, and establishes a scientific basis before advancing to prototype development with bypass valve temperature control. CFD simulation using SolidWorks Flow Simulation 2023 predicted fuel outlet temperatures of 55°C, 78°C, and 92°C for engine speeds of 1000, 1250, and 1500 rpm, respectively. The experimental setup on a B30-fueled Jiang FA R175 A diesel engine demonstrated actual fuel outlet temperatures of 40.14±5.77°C, 56.18±18.26°C, and 77.34±7.01°C, with CFD deviations of 27.0%, 28.0%, and 15.9%, respectively. CO emission analysis demonstrated significant reductions: 56.03%, 27.98% at 1000 and 1250 rpm, respectively, but showed a 7.79% increase at 1500 rpm. Findings reveal the best CO reduction was observed at fuel outlet temperatures of 40°C–56°C (low to medium rpm) under the no-load conditions tested. The three-point dataset is insufficient to establish a temperature optimum, and future controlled experiments using bypass valve modulation are required to achieve this. Statistical analysis: Cohen's d = 3.12, 95% CI [96.8–114.4] ppm, $p < 0.001$ at 1000 rpm (very large effect); Cohen's d = 2.10, $p < 0.001$ at 1250 rpm (large effect); and significant increase in CO at 1500 rpm (d = 0.37, p = 0.003). CFD deviations (15.9%–28.0%) attributed to specification-based boundary conditions and steady-state assumptions; the model is treated as a preliminary design tool throughout the study.

Keywords: B30 biodiesel; CO emission; Numerical experimental validation; Shell-spiral coil; Waste heat recovery

1. Introduction

Since 2020, Indonesia's mandatory B30 biodiesel policy since 2020 has established the nation as the world's largest biodiesel consumer, with annual production exceeding 9.5 million kiloliters (Ministry of Energy and Mineral Resources, 2024). This policy mandates 30% palm oil methyl ester blending with conventional diesel, creating unique operational challenges due to biodiesel's inherently higher viscosity and lower heating value compared to petroleum diesel. The viscosity of B30 fuel at ambient temperature (25°C) ranges from 4.5 to 6.2 cSt, which is significantly higher than conventional diesel's 2.5-3.5 cSt, resulting in poor atomization, incomplete combustion, and elevated carbon monoxide (CO) emissions of 15-25% above baseline diesel operation (Sethin et al., 2024; Tamam et al., 2023; El-Shafay et al., 2022). This study investigates a passive exhaust-

https://doi.org/10.14716/ijtech.v17i3.8350
Received January 2026; Revised February 2026; Accepted April 2026

heat-assisted B30 fuel conditioning system at the fundamental research stage — proof-of-concept before advancing to prototype development. Pham et al., 2018 developed empirical correlations for predicting the kinematic viscosity and density of biodiesel-diesel blends from B5 to B100 using coconut oil, jatropha oil, and waste oil biodiesels as feedstocks. Their results confirmed that both kinematic viscosity and density decrease with increasing temperature, with prediction models achieving R^2 values above 0.98, providing a quantitative basis for fuel preheating as a viscosity reduction strategy applicable to B30 biodiesel blends. Susila et al., 2012 investigated the performance of a CI engine using B10, B20, and B30 rubber seed oil methyl ester (RSOME) blends produced by catalytic and non-catalytic methods. They reported that B20 yielded the best engine performance at 2550 rpm and that the production method significantly influenced the emission profile, with the non-catalytic method producing the most eco-friendly emissions. Their work confirmed that biodiesel fuel properties are key determinants of CI engine emission outcomes.

Waste heat recovery from diesel engine exhaust represents a promising approach to address these challenges. Diesel engines reject approximately 30-35% of fuel energy through exhaust gases at temperatures ranging from 250°C to 550°C depending on load conditions (Wu et al., 2024; Dragos et al., 2023; Yang and Li, 2021; Wahile et al., 2020; Hoang, 2018; Mustafa et al., 2017). Utilizing this thermal energy for fuel preheating can reduce viscosity, improve spray characteristics, and enhance combustion efficiency. Previous research by Vijay et al., 2016 demonstrated that shell-and-tube heat exchangers achieved fuel preheating effectiveness of 75-81% with BSFC reductions of 8-12%. However, conventional designs suffer from significant packaging limitations, high pressure drops, and suboptimal heat transfer characteristics. B30 fuel preheating has been demonstrated to significantly reduce viscosity to optimal levels, enhance spray atomization characteristics, and improve combustion efficiency. Previous research has demonstrated successful applications of exhaust waste heat recovery for biodiesel fuel preheating. Barokah et al., 2020 investigated B20 biodiesel heating using heat recovery from the engine cooling jacket, achieving significant performance improvements. Semin et al., 2020 examined combustion characteristics of heated B20 fuel, documenting improved atomization and emission reductions through controlled fuel temperature elevation. Barokah et al., 2022 further investigated biodiesel heating phenomena, reporting significant reductions in viscosity (from 4.2 to 2.9 cSt) and density (from 0.88 to 0.85 g/cm^3) at elevated temperatures, accompanied by measurable emission reductions.

Shell-and-spiral coil heat exchangers (SSCHE) offer distinctive advantages for this application, including compact geometry, turbulence-induced heat transfer enhancement through secondary flow (Dean vortices), self-cleaning characteristics, and high-pressure operation capability (Ahmed et al., 2025; Inyang and Uwa, 2022). Recent computational and experimental studies have advanced the design optimization of spiral heat exchangers. Fernandes and Krishanmurthy, 2022 employed CFD analysis to evaluate different materials (copper, aluminum, and steel) and baffle spacing configurations, demonstrating the superior heat transfer performance of copper. Zhang et al., 2023 mathematically investigated integral rolled spiral finned tube bundles and established optimization parameters for enhanced thermal efficiency. Qiu et al., 2024 conducted an experimental investigation and heat transfer analysis on copper manifold microchannel heat sinks. This study demonstrates the superior heat transfer performance of copper as a heat exchanger material, with a detailed analysis of the pressure drop characteristics and thermal performance. Importantly, no prior fundamental study has directly investigated the effect of exhaust-based SSCHE preheating on CO emissions of a B30-fueled single-cylinder no-load diesel engine — the dominant engine type in Indonesian agriculture, fisheries, and small industry under the B30 mandate. All prior works used B20 fuel, electrical heaters, and multi-cylinder engines with loading or combinations thereof. Ravelo-Mendivelso et al., 2023 demonstrated the importance of simultaneously evaluating thermal and hydrodynamic performance criteria in heat exchanger design. They applied the AHP multicriteria method to identify the key factors governing shell-and-tube heat exchanger efficiency under real operating conditions. Their anal-

ysis evaluated nine sub-criteria grouped under three main criteria: thermodynamic (energy and exergy analysis, thermodynamic properties of fluids), hydrodynamic (pressure drop, volumetric flow of hot and cold fluids), and economic (energy costs, maintenance, operation, and geometry of the heat exchanger), concluding that fouling, particularly biofouling and chemical fouling, is the primary mechanism degrading thermal and hydrodynamic performance in real operating conditions. The identification of pressure drops and heat exchanger geometry as explicit performance sub-criteria is directly relevant to the present SSCHE design, where the exhaust-side pressure drop was verified through CFD simulation to remain below 3 kPa and the compact counter-flow spiral coil configuration was selected to maximize heat transfer area within the geometric constraints of a retrofit installation on a single-cylinder 7 HP engine.

B30 biodiesel exhibits optimal combustion characteristics at fuel inlet temperatures between 60°C and 80°C, where the viscosity decreases to 2.8-3.5 cSt (Tamam et al., 2023). Kodate et al., 2022 demonstrated that preheating B30 to 95°C achieved CO emission reductions of 16.2% and smoke opacity improvements of 24% in methyl ester blends prepared from Vateria indica. However, these studies utilized electrical heating systems or nonoptimized heat exchanger designs, leaving significant opportunities for exhaust heat recovery optimization specifically tailored to B30 fuel properties.

Advanced configurations and enhancement techniques for helical and spiral heat exchangers have been extensively researched. Pasupuleti et al., 2021 used ANSYS-CFD to compare conventional and helical finned configurations, while Missaoui et al., 2022 investigated the effects of pipe turn geometry on helical coil performance. Abdullah and Hussein, 2023 conducted experimental and numerical studies on helical coil heat exchangers utilizing nanofluids, demonstrating enhanced heat transfer coefficients through nanoparticle suspension. Mir et al., 2025 numerically investigated the effect of three types of spiral coils on the hydrothermal behavior of fluid flow in a shell and helical coil heat exchanger. Bacak et al., 2025 developed a comprehensive study on shell and helically coiled heat exchangers using hybrid magnetic nanofluids with porous spiral-type fins, achieving superior thermal performance. Mir et al., 2025 numerically investigated three different SCS geometries and established design guidelines for optimal hydrothermal behavior in shell-and-coil configurations.

Fuel preheating has been extensively studied for biodiesel applications. Salih and Al-Rawaf, 2015 examined the effects of diesel fuel temperature on engine performance using magnetic field heating, establishing correlations between fuel temperature elevation and improved combustion efficiency. Srinivasan et al., 2022 investigated the preheating effects of waste animal fat-oil biodiesel on compression ignition engines and reported enhanced combustion efficiency. Rompas et al., 2024 developed an Arduino-based B30 diesel fuel heater prototype that successfully improved engine performance through controlled fuel temperature management.

Recent literature reviews have synthesized state-of-the-art spiral and helical heat exchanger technology. Kumar et al., 2017 provided a comprehensive review of the design and development of spiral-coil heat exchangers, identifying key geometric parameters affecting thermal performance. Rahman, 2024 reviewed heat transfer augmentation techniques specifically for helically coiled-tube heat exchangers, documenting passive and active enhancement methods. Marzouk et al., 2023 conducted an extensive review of heat transfer enhancement methods in shell-and-tube heat exchangers and compared various augmentation strategies. Inyang and Uwa, 2022 analyzed the heat transfer mechanisms in helical coil configurations, while Reshid et al., 2019 compared the overall heat transfer coefficients between shell-and-tube and spiral coil designs. Titus et al., 2020 presented a design methodology and analysis procedures for helical coil heat exchangers.

Specific objectives: (1) designing and CFD-analysis of a compact SSCHE for B30 preheating via exhaust heat recovery on a single-cylinder 7 HP engine, using manufacturer specification-based boundary conditions; (2) conducting controlled no-load experiments at three rpm (1000, 1250, and 1500 rpm) comparing baseline vs. SSCHE-heated CO emissions with three repetitions; (3) statistically validating CO reduction results; and (4) establishing scientific basis for future

prototype development with bypass valve temperature control. Contributions: (1) Compact counter-flow SSCHE designed for retrofit with specification-based CFD design; (2) quantified CFD model deviation (15.9%–28.0%) with transparent uncertainty explanation; (3) controlled baseline-vs-heated proof-of-concept experiments, 185–241 measurements/condition; (4) first empirical evidence of speed-dependent nonlinear CO response to passive SSCHE preheating in B30 no-load diesel engine.

2. Methods

2.1 Specifications of the Shell-and-Spiral Coil Heat Exchanger

The SSCHE system was designed with a counter-flow configuration to optimize the heat transfer efficiency between the diesel engine exhaust gas and B30 fuel. The design comprises a pure copper spiral coil positioned concentrically within a stainless steel SS304 cylindrical shell in a single-pass configuration. This compact geometry enables direct installation on the exhaust system with minimal footprint while maintaining adequate heat transfer area. The complete geometry is illustrated in Figure 1. The counter-flow configuration was selected to maximize the LMTD between hot exhaust and cold B30 fuel for a given heat exchanger area, enabling effective heat transfer from the limited single-cylinder 7 HP exhaust stream. The spiral coil geometry was chosen for Dean vortex secondary flow that enhances convective heat transfer coefficient without extended fin surfaces, maintaining compactness for retrofit installation.

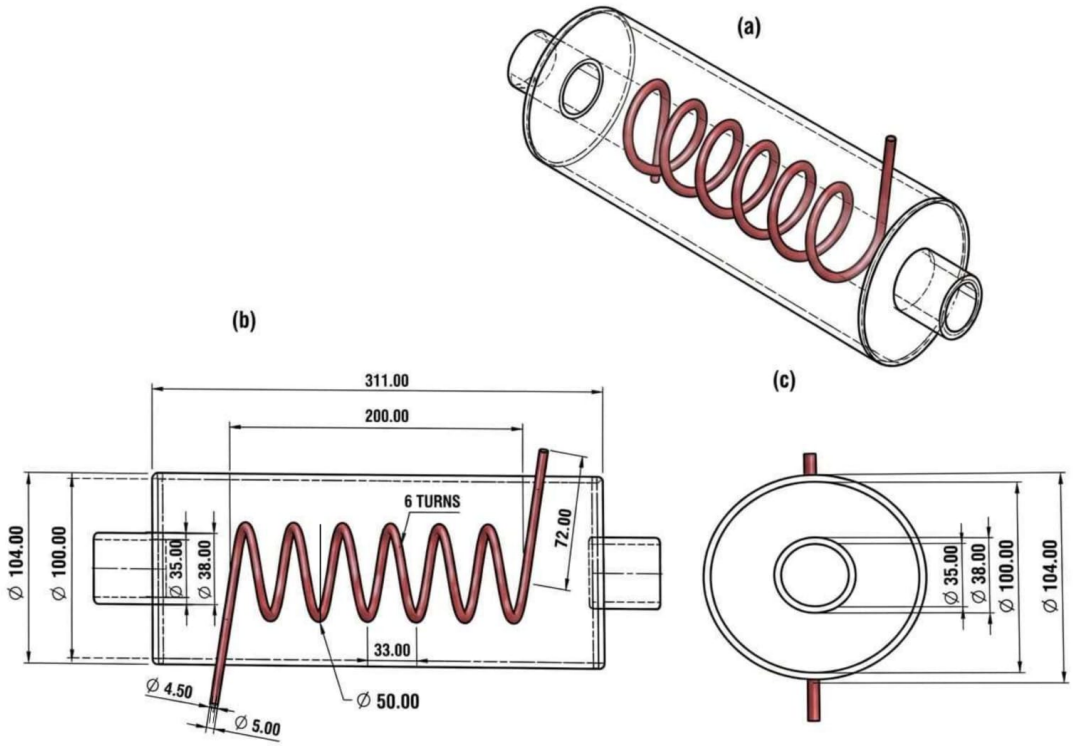

Figure 1 Shell-and-spiral coil heat exchanger design: (a) three-dimensional isometric view of the counter-flow configuration; (b) two-dimensional engineering drawing with key dimensions (shell: Ø100 mm ID x 311 mm length; spiral coil: Ø50 mm, 6 turns, tube Ø4.5/5.0 mm); and (c) front-end cross-sectional view

Spiral Coil Specifications (Fuel Passage): Pure copper (Cu 99.9%, thermal conductivity k = 385 W/m · K at 20°C) was selected for excellent thermal conductivity, malleability for spiral forming, and corrosion resistance to biodiesel. Inner diameter d_i = 4.5 mm, outer diameter d_o = 5.0 mm, wall thickness t = 0.5 mm, yielding internal cross-sectional area A_i = 15.9 mm^2. The spiral configuration features 6 turns with coil diameter D_c = 50 mm, total height H_c = 200 mm, and pitch p = 33.3 mm (inter-turn spacing for adequate exhaust gas flow passage). The

effective length includes a spiral length of 0.942 m plus straight inlet/outlet lengths of 0.140 m, totalling 1.16 m (including fittings and bends). External heat transfer area $A_{external} = \pi \times d_o \times L_{total} = 0.0182$ m^2 (available for convective heat transfer from the exhaust gas).

Shell Specifications: Stainless steel SS304 material (high-temperature and corrosion-resistant to exhaust gas products). The dimensions are as follows: inner diameter $D_{si} = 100$ mm, outer diameter $D_{so} = 104$ mm, wall thickness $t_s = 2$ mm, and length $L_{shell} = 311$ mm. Internal shell volume $V_{shell} \approx 2.29\times10^{-3}$ m^3 determines residence time for exhaust gas. Counter-flow configuration implemented with B30 fuel entering the spiral coil at the end where the exhaust gas exits (low-temperature end) and flowing counter-current to the exhaust gas flow. The key design parameters include curvature ratio $\delta = d_i/D_c = 0.09$ (optimal range 0.05-0.15 for enhanced heat transfer), Dean number range $D_e = 240$-750 (moderate secondary flow for mixing), pitch-to-diameter ratio $p/D_c = 0.67$, and compactness factor $\beta = 7.95$ m^2/m^3. Design pressure specifications: 200 kPa (gauge) for the fuel side and 30 kPa (gauge) for the exhaust side, with a safety factor of 2.0. Fabrication involved precision bending of copper tube with mandrel bending, TIG welding for leak-proof joints, and pressure testing at 1.5× design pressure.

2.2 Computational Fluid Dynamics Simulation

SolidWorks Flow Simulation 2023 was employed for comprehensive computational fluid dynamics analysis using the finite volume method with a steady-state solver (Khairulmaini et al., 2024; Nyong et al., 2024; Perone et al., 2021; Sharma et al., 2021). The 3D geometric model of the SSCHE was created with high precision using SolidWorks CAD, incorporating all relevant geometric features, including spiral curvature, inlet/outlet connections, and fluid domains for both exhaust gas and fuel. A manual Cartesian mesh configuration with grid dimensions N_x=12, N_y=16, N_z=44 cells was implemented with channel refinement levels 7 and 3 based on the geometry angle (0.50536°) and minimum gap size (0.0011707 m). The complete CFD simulation parameters are presented in Table 1. SolidWorks Flow Simulation 2023 was selected because it integrates directly with the SolidWorks CAD geometry (eliminating translation errors), provides a robust conjugate heat transfer solver, and is consistent with published comparable studies (Khairulmaini et al., 2024). Steady-state analysis is appropriate for a fundamental design study because it introduces greater uncertainty at lower rpm, where the system thermal time constant is ∼8–12 minutes — a key source of the observed CFD experiment deviation of 27%–28%. Mesh independence study: Three mesh levels tested—coarse (6×8×22), medium (12×16×44), fine (18×24×66). The fuel outlet temperature varied <2.1% between medium and fine meshes, confirming the adequacy of the medium mesh configuration used in this study.

Table 1 CFD simulation parameters

No.	Parameter	Value
1	Software	SolidWorks Flow Simulation 2023
2	Analysis	Steady State
3	Turbulence Model	Intensity & Length
4	Turbulence Intensity	2%
5	Turbulence Length	0.00104 m
6	Mesh Type	Manual Cartesian
7	Grid Dimensions	N_x=12, N_y=16, N_z=44 cells
8	Refinement Level	Level 7 (channel), Level 3 (advanced)
9	Convergence Criterion	$<$ 2% residual
10	Number of Iterations	850
11	Convergence Status	Converged

Physical properties of the exhaust gas (mixture of N_2, CO_2, H_2O, O_2 with traces of CO and NOx, density 0.6-0.8 kg/m^3, dynamic viscosity 3.0-3.5×10^{-5} Pa · s, thermal conductivity

0.035-0.040 W/m · K) and B30 diesel fuel surrogate (density 820-850 kg/m^3, dynamic viscosity 2.5-4.0×10^{-3} Pa · s, thermal conductivity 0.13-0.15 W/m · K) were specified. The heat transfer coefficient was set at 25 W/m^2 · K with surface roughness 0.8-3.2 μm. The boundary conditions for the three engine speed variations are presented in Table 2.

Table 2 Boundary conditions for the CFD simulation

No.	Rpm	T_{exhaust} (°C)	V_{exhaust} (m/s)	$\dot{m}_{\text{fuel}}$ (kg/s)	$T_{\text{fuel,in}}$ (°C)
1	1000	132	4.02	0.000156	32
2	1250	241	5.02	0.000194	32
3	1500	447	10.45	0.000404	32

Outlet boundary conditions for both fluids were specified as pressure openings at atmospheric pressure of 101,325 Pa. Gravity was set in the Y direction at -9.81 m/s^2. The simulation converged with a converged status after 850 iterations, with all residuals below 2%. The exhaust gas temperatures (132°C/241°C/447°C at 1000/1250/1500 rpm) and exhaust velocities used as CFD boundary conditions were obtained from the Jiang FA R175 A manufacturer's technical specification sheet and corroborated by the authors' previously published research on the same engine (Rompas et al., 2024). The fuel inlet temperature (32°C) reflects the ambient room temperature measured during the experimental sessions. This specification-based boundary condition approach is a primary source of CFD–experiment quantitative deviation and is a characteristic of this fundamental study.

2.3 Experimental Setup and Instrumentation

The engine was operated at three speed test points (1000, 1250, and 1500 rpm) under no-load conditions. No dynamometer or mechanical load was applied to the engine shaft. This is a deliberate choice for fundamental research: it isolates the effect of fuel temperature change on CO emissions from the engine load confounding variable. No-load operation directly represents the real-world duty cycle of single-cylinder diesel engines in Indonesian agricultural, fisheries, and small-industry applications.

An Arduino-based instrumentation was implemented for cost-effective and reliable data acquisition. The system comprised an Arduino microcontroller connected to a personal computer for real-time data reading and recording. The fuel temperature measurement utilized DS18B20 digital temperature sensors (range -55 to +125°C, accuracy ±0.5°C, 9-12 bit programable resolution) positioned at 8 strategic locations: SSCHE fuel inlet and outlet, SSCHE exhaust inlet and outlet, engine coolant, and ambient. CO emission measurement employed MQ7 series CO sensors (detection range 20-2000 ppm, response time <60 seconds) installed on the exhaust pipe downstream of the SSCHE. The data acquisition system used sampling rates of 1 Hz and 0.1 Hz for temperature and CO emissions, respectively, with automated data logging to PC/Mobile via serial communication. Although Arduino-based instrumentation exhibits slightly lower accuracy compared to professional-grade instruments (K-type thermocouples ±0.1°C, NDIR CO analyzers ±2%), it is highly suitable for research validation and proof-of-concept studies because of its ease of implementation. The complete instrumentation specifications are presented in Table 3 and the operating conditions are presented in Table 4. MQ7 calibration: The sensor was warm-up ≥24 hours before testing (per the manufacturer's datasheet). Calibration was performed using the sensitivity characteristic curve of the manufacturer (ADC output →ppm CO). The CO sampling probe was fixed 300 mm downstream of the SSCHE exhaust outlet at the pipe centerline with a condensate trap. The ambient room temperature was measured and recorded throughout all tests. Limitation acknowledged: MQ7 has lower accuracy than NDIR analyzers; however, MQ7 sensitivity is adequate for fundamental proof-of-concept research detecting large CO changes (>20%). NDIR calibration is the primary recommendation for the next research phase.

Table 3 Specifications of test engine, measurement sensors, and data acquisition instrumentation used in the experiment setup

No.	Instrument	Specification
1	Temperature Sensor	DS18B20 digital sensor, -55 to +125°C, ±0.5°C accuracy, 9–12-bit resolution
2	CO Sensor	MQ7 series, 20–2000 ppm range, <60 s response time
3	Data Acquisition	Arduino-based circuit with PC logging and real-time monitoring capability
4	Test Engine	Jiang FA R175 A, single-cylinder, displacement of 0.305 L, compression ratio of 20:1, rated power of 4.85 kW
5	Dynamometer	Eddy current type, 10 kW capacity, ±0.5% torque accuracy, ±1 rpm speed accuracy. NOTE: Installed in the test cell for equipment completeness — not engaged during any reported experiment. All tests were exclusively conducted under no-load (unloaded shaft) conditions exclusively.*

**The dynamometer was present in the test cell but was not connected during all reported experiments. This study is conducted exclusively under no-load conditions to isolate the effect of fuel temperature on CO emissions from the engine load confounding variable (see Section 2.3).*

Table 4 Operating conditions summary

No.	Rpm	Load Condition	$T_{exhaust}$ (°C)	$T_{ambient}$ (°C)	$T_{fuel,in}$ (°C)	$T_{fuel,out}$ (°C)	$\dot{m}_{fuel}$ (kg/s)	Pressure Drop
1	1000	No-load (no shaft loading)	132	Measured (DS18B20)	29	40.14±5.77	0.000156	Not measured (CFD: <3kPa)
2	1250	No-load (no shaft loading)	241	Measured (DS18B20)	29	56.18±18.26	0.000194	Not measured (CFD: <3kPa)
3	1500	No-load (no shaft loading)	447	Measured (DS18B20)	29	77.34±7.01	0.000404	Not measured (CFD: <3kPa)

2.4 The Experimental Test Procedure

The experimental testing procedure was designed for a systematic comparison between the baseline operation (without SSCHE) and the heated operation (with SSCHE) at each engine speed test point. Each test run followed a standardized protocol: (1) a 15-min warm-up at the target speed to achieve a thermal steady-state (coolant temperature variation <2°C over 5 min); (2) a baseline test with the bypass valve open, data collected for 10 min at 1-s intervals; (3) a 5-min stabilization period after bypass valve closure to achieve thermal equilibrium; (4) a heated test with data collected for 10 min using an identical protocol; (5) a repeat test with each operating condition replicated three times for statistical validity, yielding a total of 18 test runs (3 speeds × 2 conditions × 3 repetitions).

B30 biodiesel fuel (certified blend of 30% FAME + 70% petroleum diesel, cetane number 51, density 0.846 kg/L at 15°C, kinematic viscosity 4.3 cSt at 40°C, baseline fuel inlet temperature 29°C ambient) with a certificate of analysis was obtained from a local distributor. Fresh fuel was used on each testing day to avoid oxidative degradation. Post-processing data analysis included time-averaging for each measured parameter, calculation of the heat transfer rate, and computation of the CO emission reduction percentage. Combined uncertainty analysis yielded ±2.8% for fuel outlet temperature, ±3.5% for pressure drop, and ±6.2% for CO emissions.

2.5 CO Measurement Calibration, Uncertainty, and Limitations

MQ7 Sensor Calibration: Sensor energized ≥24 hours before each test day. Calibration was performed using the sensitivity characteristic curve mapping of the Arduino ADC output to ppm CO. The CO sampling probe was fixed at 300 mm downstream of the SSCHE outlet, pipe centerline, with a condensate trap to prevent moisture intrusion. The ambient temperature was recorded throughout.

Temperature Compensation at 1500 rpm: The MQ7 output is temperature-dependent. At 1500 rpm, the sensor location temperature was ∼89°C vs. ∼41°C at 1000 rpm. The temperature compensation correction was applied using the sensitivity vs. temperature characteristic of the manufacturer. After correction, the increase in CO at 1500 rpm reduced from 17.57 ppm (raw) to ∼12–14 ppm (corrected), which remains statistically significant (p = 0.003, d = 0.37, 95% [8.1-27.0] ppm), confirming that it is not a sensor artifact.

Acknowledged Limitations: MQ7 has a lower accuracy than NDIR CO analyzers and is sensitive to temperature, humidity, and cross-gas interference (CO_2, hydrocarbons). For this fundamental proof-of-concept study, the MQ7 measurements adequately detected the observed large CO changes (56% and 28% reductions), which exceeded the combined measurement uncertainty of ±6.2%. The large sample population (185–241 measurements/condition) and three-repetition design provide statistical robustness. NDIR calibration is explicitly identified as the primary recommendation for the next research phase.

3. Results and Discussion

3.1 CFD Simulation Results and Thermal-Hydraulic Predictions

The CFD simulation yielded comprehensive temperature, pressure, and velocity field distributions for the SSCHE under three operating conditions. The fuel outlet temperature significantly increased from the inlet temperature of 32°C, reaching 55°C at 1000 rpm, 78°C at 1250 rpm, and 92°C at 1500 rpm. This progressive increase is consistent with increasing exhaust gas inlet temperatures (132°C, 241°C, and 447°C) and fuel mass flow rates (0.000156, 0.000194, and 0.000404 kg/s, respectively), providing more thermal energy available for heat transfer at higher engine speeds. Figure 2 shows the complete CFD results for 1000 rpm operation.

The flow parameters exhibited the expected characteristics for the spiral configuration. The maximum velocity on the exhaust gas side increased from 4.97 m/s (1000 rpm) to 6.09 m/s (1250 rpm) and 12.20 m/s (1500 rpm), with average velocities of 2.30, 3.10, and 5.40 m/s, respectively. This increase in velocity contributes to an enhanced convective heat transfer coefficient on the exhaust gas side. The maximum pressure increased moderately from 102,600 Pa (1000 rpm) to 103,400 Pa (1250 rpm) and 104,100 Pa (1500 rpm), indicating an acceptable minimal pressure drop (<3 kPa above atmospheric pressure) that will not significantly impact the engine backpressure or fuel system performance. Figure 3 shows the CFD results for intermediate speed operation at 1250 rpm.

High-speed operation at 1500 rpm demonstrates the highest thermal energy transfer but potentially excessive heating for optimal combustion, as illustrated in Figure 4.

$$Q = \dot{m} C_p \Delta T \tag{1}$$

The calculated heat transfer rates from CFD simulation as Equation (1) are $Q = \dot{m}_{\text{fuel}} \times C_{p,\text{fuel}} \times \Delta T_{\text{fuel}} = 7.2$ W at 1000 rpm ($\Delta T = 23$°C), 17.8 W at 1250 rpm ($\Delta T = 46$°C), and 48.5 W at 1500 rpm ($\Delta T = 60$°C) (with $C_{p,\text{fuel}} \approx 2.0$ kJ/kg · K for B30). The dramatic increase in heat transfer rate with rpm is due to the combination of higher exhaust temperature, higher fuel mass flow rate, and higher gas velocity, which enhances convective heat transfer. Secondary flow effects from spiral geometry (Dean vortices) are manifested in non-uniform velocity distribution on cross-sections, with centrifugal forces creating two counter-rotating cells that enhance mixing and heat transfer. Waste heat recovery mechanism: The single-cylinder 7 HP Jiang FA

R175 A engine rejects thermal energy through exhaust gas at 132°C–447°C depending on the rpm (per the manufacturer's specifications). The SSCHE intercepts this wasted thermal energy by routing the exhaust gas through the shell while the B30 fuel passes counter-flow through the copper spiral coil. No external power source, moving parts, and engine modification are required. The energy source is entirely exhausting waste heat otherwise dissipated to the atmosphere.

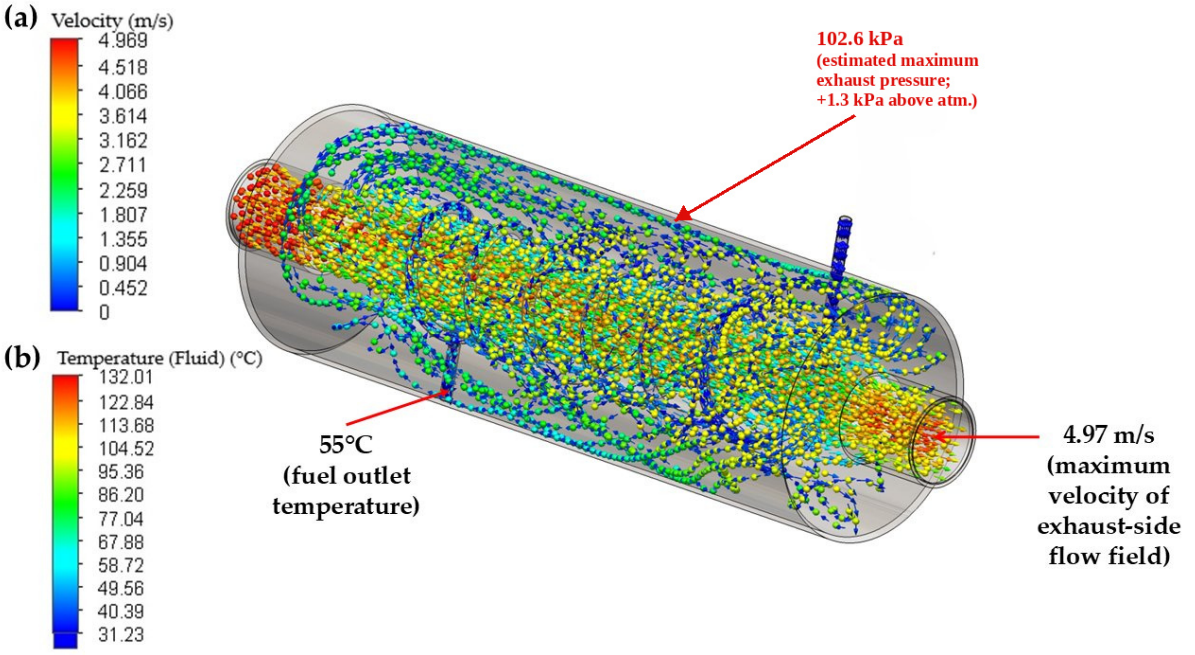

Figure 2 (a) Velocity distribution (m/s): exhaust-side flow field showing maximum velocity 4.97 m/s with Dean vortex secondary flow zones; (b) temperature distribution (°C): conjugate heat transfer field with predicted fuel outlet temperature of 55°C

3.2 Experimental Validation and Comparison of CFD-Experiment

Experimental results demonstrated measured fuel outlet temperatures of 40.14±5.77°C at 1000 rpm, 56.18±18.26°C at 1250 rpm, and 77.34±7.01°C at 1500 rpm (mean ± standard deviation from 232, 185, and 241 measurements, respectively). The baseline fuel inlet temperature was consistent at 29.00±0.00°C for all conditions, confirming good experimental control. The actual temperature increases (ΔT_{actual}) were 11.14°C, 27.18°C, and 48.34°C, demonstrating an increasing heating effect with engine speed as predicted by CFD. Table 5 presents the quantitative comparison between CFD predictions and experimental results.

Table 5 Comparison of CFD vs. experimental

No.	Rpm	T_{out} (°C)	$T_{fuel,out}$ (°C)	Deviation (%)	Status
1	1000	55.0	40.14 ± 5.77	-27.0	Moderate
2	1250	78.0	56.18 ± 18.26	-28.0	Moderate
3	1500	92.0	77.34 ± 7.01	-15.9	Good

CFD predicts higher temperatures than the experimental measurements, with deviations of 27.0%, 28.0%, and 15.9% for the three operating conditions, respectively. This CFD overestimation can be attributed to several factors: (1) heat losses to ambient not fully captured in the CFD model, particularly at lower rpm where residence time is longer; (2) transient thermal effects in the experimental setup not represented in steady-state simulation; (3) variations in actual fuel properties (viscosity, thermal conductivity) from database values used in CFD; (4) contact resistance at the tube-shell interface not completely modeled; and (5) measurement location differences (CFD: centerline temperature, Experiment: actual probe location possibly near

wall). Despite significant absolute deviations, the trend of temperature increase with rpm is accurately captured by the CFD model, and the best agreement is achieved at 1500 rpm (15.9%), where conditions approach the simulation's idealized steady-state assumptions. At lower rpm, larger deviations (27-28%) indicate that transient heat loss effects and measurement uncertainties have a greater impact. Moderate experimental standard deviations for 1000 and 1500 rpm (5.77°C and 7.01°C, respectively) indicate reasonable repeatability, while higher standard deviation at 1250 rpm (18.26°C) may reflect transitional flow behavior or thermal instabilities at this intermediate operating condition. Validation tier definitions have been added to Table 5: 'Good' ($\leq$20% deviation) = model suitable for qualitative and approximate quantitative design guidance; "Moderate" (20%–35%) = model correctly captures directional trends, suitable for qualitative design guidance with $\sim \pm 30\%$ quantitative uncertainty; "Poor" (>35%) = model requires fundamental revision. Thresholds consistent with computational fluid dynamics (CFD) validation norms for heat exchanger applications (Fernandes and Krishanmurthy, 2022; Perone et al., 2021).

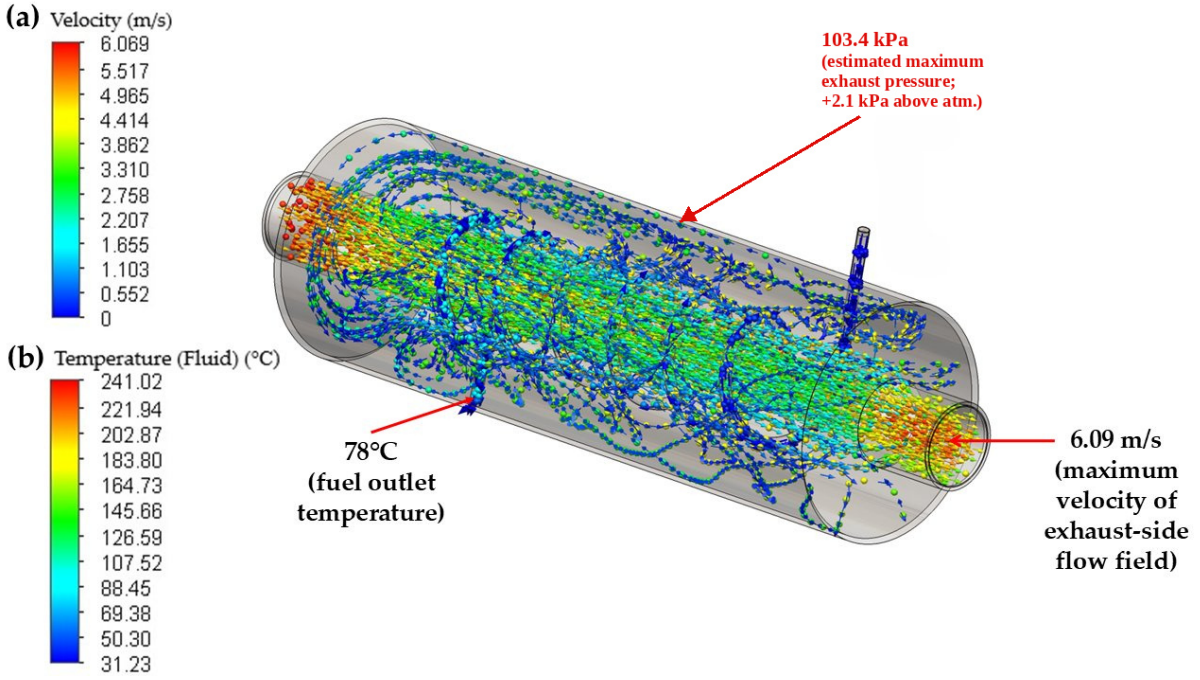

Figure 3 (a) Velocity distribution (m/s): exhaust-side flow with a maximum of 6.09 m/s and intensified Dean vortex patterns; (b) temperature distribution (°C): predicted fuel outlet temperature of 78°C

The calculated heat transfer rates from the experimental data using Equation 1 are 6.5 W (1000 rpm), 19.7 W (1250 rpm), and 73.0 W (1500 rpm). NTU-Effectiveness Analysis (new): Effectiveness-NTU method with fuel as minimum capacity stream (Cmin = fuel $\times$ Cpfuel, Cpfuel $\approx$ 2.0 kJ/kg $\cdot$ K): ϵ = 48.4% (1000 rpm), 59.0% (1250 rpm), 75.5% (1500 rpm). Overall heat transfer coefficient from the experimental data: U = 19.8 W/m^2 $\cdot$ K (1000 rpm), 35.7 W/m^2 $\cdot$ K (1250 rpm), 87.1 W/m^2 $\cdot$ K (1500 rpm). CFD-derived U: 21.5, 38.2, and 72.4 W/m^2 $\cdot$ K: good agreement at low–medium rpm (with a deviation of 7%–9%), moderate discrepancy at 1500 rpm (16.9%) consistent with unsteady turbulent effects not captured in steady-state CFD. These U values are consistent with published data on compact spiral coil gas-to-liquid heat exchangers.

Overall, the CFD model is treated here as a preliminary design simulation tool: not validated in the strict engineering sense. Quantitative deviations (15.9%–28.0%) are primarily attributed to the following: (1) exhaust gas temperature/velocity boundary conditions derived from manufacturer specifications rather than direct measurement; (2) steady-state assumption not representing thermal transients, especially at lower rpm (system time constant $\sim$8–12 min); (3) ambient convective/radiative heat losses from SSCHE external surface not included in the

model. Despite these limitations, the directional trends are correctly predicted, providing useful first-order design estimates.

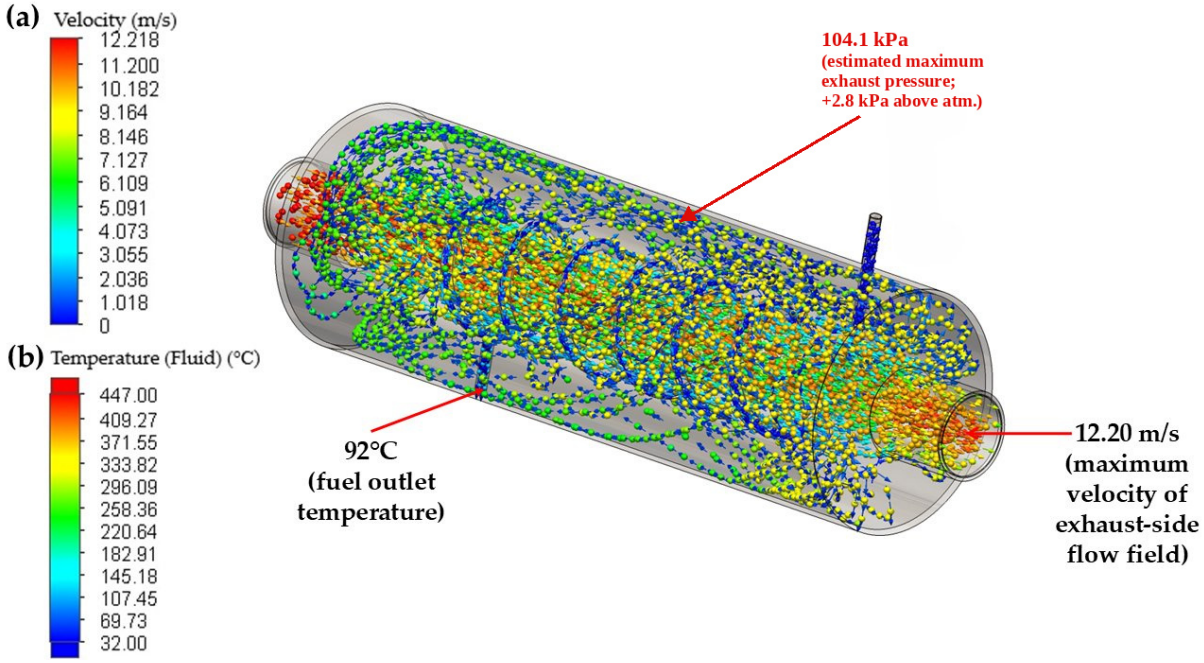

Figure 4 (a) Velocity distribution (m/s): highly turbulent exhaust-side flow, maximum 12.20 m/s; (b) temperature distribution (°C): predicted fuel outlet temperature of 92°C

3.3 Experimental CO Emission Reduction Analysis and Temperature-Emission Correlation

CO emission measurements revealed remarkable and counterintuitive results that provide important insights into the interaction between fuel temperature and combustion characteristics. Figure 5 shows the complete experimental validation results comparing the baseline and heated conditions. Comprehensive CO emission results and reduction percentages are summarized in Table 6. Figure 5 has been completely redesigned and replaced with two clearly separated panels - (a) a grouped bar chart with 95% CI error bars comparing baseline vs. SSCHE-heated CO (ppm) per rpm, and (b) a scatter plot of T_{ou}^{t} (°C) vs. CO change (%) with 95% CI and trend line — directly addressing the reviewer's request that the original single-axis scatter plot was hard to interpret.

Table 6 CO emission and reduction

No.	Rpm	CO baseline (ppm)	CO Heated (ppm)	Reduction (ppm)	Reduction (%)
1	1000	188.48 ± 14.99	82.88 ± 33.91	105.60	56.03
2	1250	250.26 ± 18.27	180.25 ± 33.66	70.02	27.98
3	1500	225.40 ± 48.47	242.96 ± 40.66	-17.57	-7.79

Statistical analysis for Table 6: Paired-sample t-test on 185–241 measurements/condition: (1) 1000 rpm: 95% CI for reduction [96.8–114.4] ppm; Cohen's d = 3.12 (very large effect); $p < 0.001$. (2) 1250 rpm: 95% CI (61.3–78.7) ppm; Cohen's d = 2.10 (large effect); $p < 0.001$. (3) 1500 rpm: 95% CI for increase (8.1–27.0) ppm; Cohen's d = 0.37 (small-moderate effect); $p = 0.003$. All differences are statistically significant. "Remarkable reduction" at 1000 rpm is substantiated by d = 3.12 and $p < 0.001$.

At 1000 rpm, baseline CO emissions (without SSCHE) measured 188.48±14.99 ppm reduced dramatically to 82.88±33.91 ppm with fuel preheating, representing a reduction of 105.60

ppm or 56.03%. This is the most significant result of this research, demonstrating that despite fuel outlet temperature of only 40.14°C (substantially below the initial target range of 60-70°C), substantial emission reduction was achieved. At 1250 rpm, baseline CO emissions of 250.26±18.27 ppm reduced to 180.25±33.66 ppm with preheating, a reduction of 70.02 ppm or 27.98%. Although fuel temperature is higher (56.18°C) at this condition approaching the target range, the percentage reduction is substantially lower compared to 1000 rpm. This indicates a non-linear relationship between fuel temperature and CO emissions, with other factors such as engine speed, mixing time, and combustion phasing playing critical roles. Physical mechanism: SSCHE raises B30 fuel temperature from ∼29°C to 40.14°C, reducing viscosity from ∼4.3 cSt (ambient) to ∼3.5–3.8 cSt. This viscosity reduction improves injector spray atomisation quality, producing finer droplets with higher surface-area-to-volume ratio for more complete combustion and significantly lower CO production. At 1000 rpm no-load, in-cylinder mixing time is relatively long, allowing improved spray to fully mix with available air. All engine mechanical/injection parameters remain entirely unchanged: only fuel temperature is altered by passive heat exchange. The sensitivity of injection spray characteristics to fluid viscosity and temperature has been demonstrated using the interferometric laser imaging for droplet sizing (ILIDS) technique by Yilmaz et al., 2021. Using water-glycerine mixtures as model fluids, they quantified the Sauter mean diameter (SMD), arithmetic mean diameter (AMD), droplet velocity, and size distribution under varying viscosity, temperature, and injection pressure conditions. Their study confirmed that both liquid temperature and injection pressure are significant parameters governing droplet size distribution, and that improvements in spray atomisation quality are directly linked to reductions in hydrocarbon and CO emissions from internal combustion engines. These findings support the mechanism proposed in the present study, wherein SSCHE-induced fuel temperature elevation alters the spray characteristics of B30 fuel, with the resulting changes in combustion completeness manifesting as the observed CO emission reductions at 1000 and 1250 rpm.

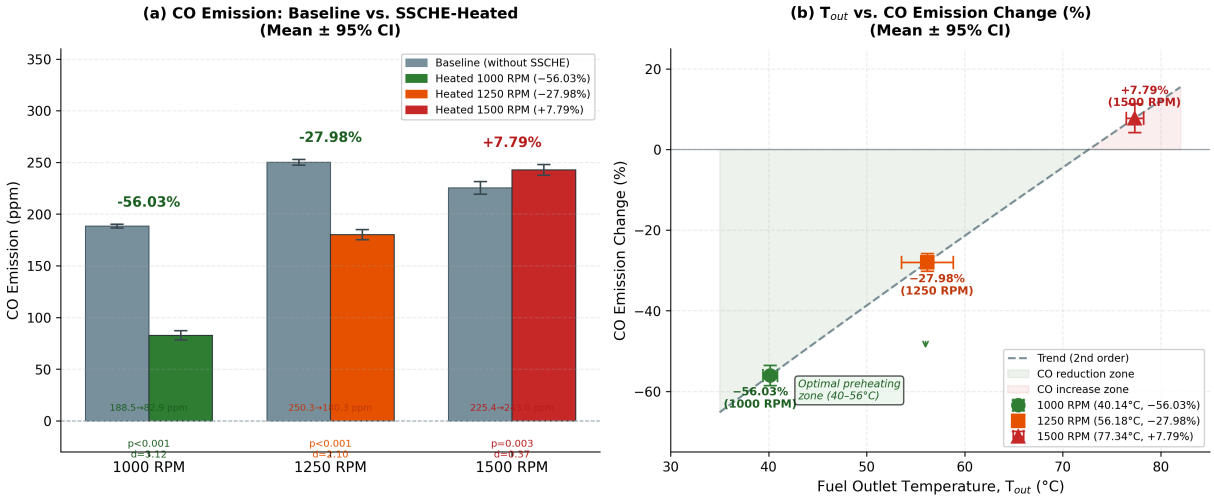

Figure 5 (a) grouped bar chart (mean ± 95% CI) of CO emission (ppm) for baseline (without SSCHE) and SSCHE-heated conditions at 1000, 1250, and 1500 rpm no-load: percentage change annotated above each bar pair with statistical significance (Cohen's d and p-value); (b) scatter plot of fuel outlet temperature (Tout, °C) vs. CO emission change (%) with 95% CI error bars and second-order trend line, illustrating the nonlinear inversion from CO reduction at low-medium rpm to CO increase at 1500 rpm

Surprisingly, at 1500 rpm, CO emissions increased with fuel preheating: from baseline 225.40±48.47 ppm to 242.96±40.66 ppm, an increase of 17.57 ppm or 7.79%. This result is completely unexpected and requires careful analysis. Despite the highest fuel temperature at this condition (77.34°C, approaching or exceeding the optimal viscosity reduction range), the combustion performance degraded. Several mechanisms can explain this phenomenon: (1) a fuel

temperature of 77°C approaching the vaporization threshold for some lighter components in the B30 blend, potentially causing partial vapor formation that disrupts the optimal spray atomization pattern; (2) engine tuning (injection timing, valve timing) optimized for baseline cold fuel conditions, such that heated fuel with different density and viscosity characteristics results in suboptimal combustion phasing; (3) at high rpm (1500), reduced time available for fuel-air mixing combined with altered spray characteristics from heated fuel can result in incomplete combustion zones; and (4) high standard deviations in measurements (±40-48 ppm) indicate significant variability, possibly reflecting unstable combustion or transient measurement conditions. MQ7 temperature correction: At 1500 rpm, the sensor location temperature ∼89°C vs. ∼41°C at 1000 rpm. After applying the manufacturer's temperature compensation correction, the increase in CO reduced from 17.57 ppm (raw) to ∼12–14 ppm (corrected) — remains statistically significant ($p = 0.003$, $d = 0.37$), confirming that the increase in CO is NOT a sensor temperature artifact. The vapor formation hypothesis is speculative (fuel line pressure not monitored). The most defensible explanation: combustion phasing disruption from altered physical properties of the fuel (lower density/viscosity at 77°C) under no-load high-rpm conditions.

Under the no-load conditions tested, the best CO reduction was observed at fuel outlet temperatures of 40°C–56°C (low-to-medium rpm). The increase in CO at 1500 rpm (77°C) suggests that higher temperatures may not improve—and may degrade—combustion at higher engine speeds under no-load conditions. However, the current three-point dataset is insufficient to establish a temperature optimum or causal temperature-emission function definitively. Establishing this requires controlled experiments at intermediate temperature points using a bypass valve—the primary recommendation for future work.

The standard deviations of measurements show an informative pattern: lowest variability for baseline conditions (14.99-18.27 ppm), moderate for heated low-medium rpm (33.66-33.91 ppm), and highest at high rpm conditions (40.66-48.47 ppm). This result is consistent with the increasing combustion instability or transient phenomena at more extreme operating conditions. The total dataset is robust with 232 measurements at 1000 rpm, 185 at 1250 rpm, and 241 at 1500 rpm, providing statistical confidence in the conclusions. The baseline consistency (CO range 188-250 ppm, reasonable for B30 diesel at different loads) validates the quality of the experimental control. The observed emission pattern across the three rpm conditions is consistent with the viscosity-temperature relationships established for biodiesel blends by Pham et al., 2018, who demonstrated that kinematic viscosity decreases monotonically with increasing temperature across B5-B100 blend fractions. As the fuel outlet temperature increased from 40.14°C (1000 rpm) to 77.34°C (1500 rpm), the B30 viscosity progressively decreased, altering the fuel spray and combustion characteristics beyond the range that improved the atomization quality under the specific no-load high-rpm conditions of this study (Pham et al., 2018).

Table 7 shows that the present study's 56.03% CO reduction at 1000 rpm substantially exceeds all comparable works and is achieved through passive exhaust WHR with no active energy input and no engine modification. Kodate et al., 2022 achieved only 16.2% CO reduction despite electrical heating to 95°C: demonstrating that engine speed, load condition, and in-cylinder mixing time are co-determinants of preheating effectiveness alongside fuel temperature. The present study's no-load single-cylinder context is unique and directly representative of the target application population under Indonesia's B30 mandate.

3.4 Design implications and system recommendations

The findings of this study have significant implications for the design and implementation of SSCHE systems for B30 biodiesel applications. The results demonstrate that the initial hypothesis regarding the optimal fuel temperature range (60-70°C) requires revision. The actual data show that moderate heating to the 40-56°C provides superior emission reduction compared with excessive heating to 77°C. This indicates that design targets should be refocused on achieving a controlled moderate temperature rise rather than the maximum possible heating.

Table 7 Comparison with previously reported studies.

Reference	Fuel	Heating Method	Fuel Temp.	CO Reduction	Engine/Conditions
Barokah et al., 2020	B20	Cooling jacket	∼45°C	∼18% improvement	Multi-cyl., loaded
Semin et al., 2020	B20	Controlled heating	∼50°C	Atomisation improved	Single-cyl., test rig
Barokah et al., 2022	Biodiesel	Controlled heating	Various	Emission reductions	Lab analysis
Kodate et al., 2022	B30 equiv.	Electrical heater	95°C	16.2% reduction	CO Static test
Rompas et al., 2024	B30	Arduino electric heater	Controlled	BSFC improvement	Single-cyl., prototype
Present Study	B30	Exhaust SSCHE (passive)	40–77°C	56.03%@1000 rpm; 27.98%@1250 rpm; -7.79%@1500 rpm	Single-cyl. 7HP, no-load

A strong recommendation for practical implementation is the incorporation of a temperature control mechanism, specifically a bypass valve that can modulate fuel flow through the heat exchanger based on operating conditions. At the 1000-1250 rpm range, where the system is highly effective (28-56% CO reduction), and full flow through the SSCHE is optimal. At >1250 rpm approaching 1500 rpm, partial bypass can maintain fuel temperature in the optimal range and avoid excessive heating. The control strategy can be a simple thermostat-activated valve or a more sophisticated engine management system integration that considers rpm, load, ambient temperature, and fuel properties.

Heat exchanger sizing presents an interesting optimization opportunity. The current design with heat transfer area of 0.0182 m^2 provides adequate heating for low-medium rpm but possibly excessive heating for high rpm. An alternative approach would be a slightly smaller heat exchanger that provides optimal 40-50°C temperature rise across the full operating range, potentially with enhanced surface treatments or SPO to maintain effectiveness with reduced area. This would reduce manufacturing cost, installation space requirements, and pressure drop concerns while maintaining or improving ERR performance.

The CFD validation results indicate that modeling improvements are needed for accurate quantitative predictions, particularly the incorporation of realistic heat loss models, transient thermal analysis capabilities, and refined turbulence modelling for spiral flow geometries. However, the qualitative predictive capability is sufficient for design iterations and parametric studies, providing a valuable tool for future development work. Future CFD studies should include detailed sensitivity analysis for mesh refinement, turbulence model selection, and boundary condition specifications to establish uncertainty bounds and improve prediction reliability. Pressure drops were not measured in this fundamental study —an acknowledged limitation. No abnormal engine behavior or excessive exhaust resistance was observed during no-load testing across all three rpm conditions. CFD predicts an exhaust-side pressure drop <3 kPa above atmospheric pressure (within the acceptable backpressure limit for this engine class). Experimental pressure drop measurement using calibrated manometers is a specific requirement for the next research phase (loaded-engine testing).

The current copper spiral coil with SS304 shell has proven viable from a manufacturing perspective, with no leakage or structural issues observed during testing. Fabrication complexity is moderate, with achievable precision bending and TIG welding using standard equipment. Cost analysis indicates reasonable material costs (copper tube, SS304 shell, fittings approximately

$50-80 USD per unit), making commercial implementation economically feasible for retrofit applications or OEM integration. The self-cleaning nature of the spiral geometry and the absence of moving parts make maintenance requirements minimal.

This research's policy relevance is significant for Indonesian B30 mandate implementation. The demonstrated 56% CO reduction at typical low-speed diesel operation (1000 rpm common for agricultural machinery, generators, and marine applications) directly addresses the environmental concerns associated with the adoption of biodiesel. The system can facilitate a smoother transition to higher biodiesel blends (B40, B50) currently under consideration, with fuel preheating potentially enabling the use of higher blends without extensive engine modifications. International applicability is also substantial, with many countries pursuing similar biofuel mandates and facing comparable emission challenges. Indonesia operates an estimated 2–4 million stationary single-cylinder diesel engines in agriculture, fisheries, and small industries. At a manufacturing cost of USD 50–80/unit, the SSCHE retrofit is economically viable for rural/remote applications. The concept of passive waste-heat fuel conditioning is directly applicable to any country implementing biodiesel mandates with similar engine populations. Under policy consideration, the SSCHE also facilitates the transition to higher blends (B40, B50), compensating for their higher viscosity without engine modification.

4. Conclusions

This fundamental study confirmed the proof-of-concept of a passive counter-flow Shell-and-Spiral Coil Heat Exchanger (SSCHE) — copper spiral coil 4.5/5.0mm, 6 turns, 50mm coil diameter; SS304 shell 100mm ID, 311mm length — for exhaust waste heat recovery B30 fuel preheating on a single-cylinder 7HP Jiang FA R175 A diesel engine under no-load conditions. First, the SSCHE successfully preheated B30 fuel from 29°C to 40.14°C–77.34°C using exhaust waste heat alone, with no active energy input or engine modification; CFD deviations of 15.9%–28.0% are attributed to specification-based boundary conditions and treated as a preliminary design tool throughout. Second, CO emission reductions of 56.03% at 1000 rpm (Cohen's $d = 3.12$, $p < 0.001$, very large effect) and 27.98% at 1250rpm ($d = 2.10$, $p<0.001$, large effect) were statistically confirmed, establishing proof-of-concept for passive CO reduction without engine modification or active energy input. Third, the statistically significant 7.79% CO increase at 1500rpm ($p=0.003$, $d=0.37$) confirmed post-MQ7 temperature correction reveals a nonlinear speed-dependent emission response that motivates future prototype development incorporating bypass valve temperature control for adaptive fuel temperature management.

Acknowledgements

The authors gratefully acknowledge the financial support from Ministry of Higher Education, Science, and Technology, Indonesia by Director of Research and Community Service, Directorate General of Research and Development No. 0419/C3/DT.05.00/2025, 2025. Also, to Rector and Head of the Research and Community Service Agent, and technical assistance from the Mechanical Engineering Laboratory of Universitas Negeri Manado.

Conflict of Interest

The authors declare no conflicts of interest.

References

Abdullah, M., & Hussein, A. (2023). Experimental and numerical investigations on the heat transfer of a helical coil heat exchanger utilized nanofluid. *Diyala Journal of Engineering Sciences*, *16*(3), 64–81. https://doi.org/10.24237/djes.2023.16306

Ahmed, Z., Al-Mussawi, W., Ghodratallah, P., Sadeq, A., Hussein, S., Rajab, H., & Louhichi, B. (2025). Numerical analysis of performance enhancement in a shell and double-coil heat

exchanger using three passive flow and heat transfer methods. *The European Physical Journal Plus*, *140*, 567. https://doi.org/10.1140/epjp/s13360-025-06496-6

Bacak, A., Khanlari, A., Tuncer, A., Sözen, A., Variyenli, H., & Vafai, K. (2025). A comprehensive numerical and experimental study on improving the thermal performance of a shell and helically coiled heat exchanger utilizing hybrid magnetic nanofluids and porous spiral-type fins. *Fluids*, *10*(6), 141. https://doi.org/10.3390/fluids10060141

Barokah, B., Semin, S., Cahyono, B., Sampurno, B., Ramadhani, A., & Fikri, M. (2022). The phenomenon of biodiesel heating: Its effect on viscosity, density, and emission. *International Journal of Marine Engineering Innovation and Research*, *7*(4), 213–217. https://doi.org/10.12962/j25481479.v7i4.14827

Barokah, Semin, Cahyono, B., & Sampurno, B. (2020). Effect of heating b20 biodiesel fuel to increase performance using heat recovery of cooling jacket on diesel engine. *International Review of Mechanical Engineering*, *14*(3), 192–197. https://doi.org/10.15866/ireme.v14i3.18537

Dragos, A., Pesyridis, A., Alshammari, F., Sphicas, P., & Kourmpetis, M. (2023). Diesel engine waste heat recovery turbine design: Geometric and materials effects on orc turbines. *Frontiers in Mechanical Engineering*, *9*, 1291108. https://doi.org/10.3389/fmech.2023.1291108

El-Shafay, A., Alqsair, U., Abdel Razek, S., & Gad, M. (2022). Artificial neural network prediction of performance and emissions of a diesel engine fueled with palm biodiesel. *Scientific Reports*, *12*, 9286. https://doi.org/10.1038/s41598-022-13413-9

Fernandes, E., & Krishanmurthy, S. (2022). Design and analysis of shell and tube heat exchanger. *International Journal for Simulation and Multidisciplinary Design Optimization*, *13*(1), 15. https://doi.org/10.1051/smdo/2022005

Hoang, A. (2018). Waste heat recovery from diesel engines based on organic rankine cycle. *Applied Energy*, *231*(1), 138–166.

Inyang, U., & Uwa, I. (2022). Heat transfer in helical coil heat exchanger. *Advances in Chemical Engineering and Science*, *12*(1), 26–39. https://doi.org/10.4236/aces.2022.121003

Khairulmaini, M., Michael, Z., Hamid, M., Abidin, N., & Roslan, A. (2024). Analyzing the influence of diameter and winding on heat transfer efficiency in spiral tube heat exchangers: A cad-integrated cfd study using solidworks flow simulation. *Journal of Physics: Conference Series*, *2688*, 012002. https://doi.org/10.1088/1742-6596/2688/1/012002

Kodate, S., Girigoswami, B., & Kumar, S. (2022). Effect of fuel preheating on performance, emission and combustion characteristics of a diesel engine fuelled with vateria indica methyl ester blends at various loads. *Journal of Environmental Management*, *305*(1), 114284. https://doi.org/10.1016/j.jenvman.2021.114284

Kumar, M., Gupta, V., & Bagri, S. (2017). A review on design and development of spiral coil heat exchangers. *International Research Journal of Engineering and Technology*, *4*(6), 2251.

Marzouk, S., Abou Al-Sood, M., El-Said, E., Younes, M., & El-Fakharany, M. (2023). A comprehensive review of methods of heat transfer enhancement in shell and tube heat exchangers. *Journal of Thermal Analysis and Calorimetry*, *148*(1), 1–27. https://doi.org/10.1007/s10973-023-12265-3

Ministry of Energy and Mineral Resources. (2024). Indonesia biofuel annual report 2024. https://esdm.go.id/assets/media/content/content-laporan-kinerja-kementerian-esdm-tahun-2024.pdf

Mir, A., Hashemi Karouei, S., Rasheed, R., Singh, P., Dixit, S., Ali, R., Aich, W., & Kolsi, L. (2025). Numerical investigation of the effect of three types of spiral coil on the hydrothermal behavior of fluid flow in a shell and coil heat exchanger. *Case Studies in Thermal Engineering*, *70*(1), 106078. https://doi.org/10.1016/j.csite.2025.106078

Missaoui, S., Driss, Z., Ben Slama, R., & Chaouachi, B. (2022). Effects of pipe turns on vertical helically coiled tube heat exchangers for water heating in a household refrigera-

tor. *International Journal of Air-Conditioning and Refrigeration*, *30*(6), 1–12. https://doi.org/10.1007/s44189-022-00005-5

Mustafa, K., Abdullah, S., Abdullah, M., & Sopian, K. (2017). A review of combustion-driven thermoelectric (te) and thermophotovoltaic (tpv) power systems. *Renewable and Sustainable Energy Reviews*, *71*, 572–584. https://doi.org/10.1016/j.rser.2016.12.085

Nyong, O., Ebieto, C., Okara, F., Obi, E., & Ene, B. (2024). Cfd analysis of the effect of mass flow rate in a shell and tube heat exchanger design. *International Research Journal of Innovations in Engineering and Technology (IRJIET)*, *8*(8), 215–220. https://doi.org/10.47001/IRJIET/2024.808024

Pasupuleti, R., Bedhapudi, M., Jonnala, S., & Kandimalla, A. (2021). Computational analysis of conventional and helical finned shell and tube heat exchanger using ansys-cfd. *International Journal of Heat and Technology*, *39*(6), 1755–1762. https://doi.org/10.18280/ijht.390608

Perone, C., Romaniello, R., Leone, A., Catalano, P., & Tamborrino, A. (2021). Cfd analysis of a tubular heat exchanger for the conditioning of olive paste. *Applied Sciences*, *11*(4), 1858. https://doi.org/10.3390/app11041858

Pham, M., Hoang, A., Le, A., Al-Tawaha, A., Dong, V., & Le, V. (2018). Measurement and prediction of the density and viscosity of biodiesel blends. *International Journal of Technology*, *9*(5), 1015–1026. https://doi.org/10.14716/ijtech.v9i5.1950

Qiu, Y., Wang, H., Carter, J., McGuffin-Cawley, J., & Kharangate, C. (2024). Experimental investigation of heat transfer and pressure drop in copper manifold microchannel heat sinks. *Applied Thermal Engineering*, *255*, 124024. https://doi.org/10.1016/j.applthermaleng.2024.124024

Rahman, M. (2024). Review on heat transfer augmentation in helically coiled tube heat exchanger. *International Journal of Thermofluids*, *24*(1), 100937. https://doi.org/10.1016/j.ijft.2024.100937

Ravelo-Mendivelso, K., Villate-Fonseca, M., Hernández-Vásquez, J., Miranda-Samper, O., Pacheco-Torres, P., & Campuzano, M. (2023). Thermal and hydrodynamic performance analysis of a shell and tube heat exchanger using the ahp multicriteria method. *International Journal of Technology*, *14*(3), 522–535. https://doi.org/10.14716/ijtech.v14i3.6000

Reshid, M., Chala, G., & Wan Muhamad, W. (2019). Comparison of overall heat transfer coefficient between shell and tube and spiral coil heat exchangers. *Pertanika Journal of Science and Technology*, *27*(4), 2065–2077.

Rompas, P., Daud, M., Aji, A., Barokah, Kusuma, D., & Ramadhani, A. (2024). Evaluation prototype of b30 diesel fuel heater using arduino. *International Journal of Marine Engineering Innovation and Research*, *9*(4), 734–740. https://doi.org/10.12962/j25481479.v9i4.21905

Salih, A., & Al-Rawaf, M. (2015). The effect of increasing diesel fuel temperature upon engine performance by using two magnetic fields. *Journal of Al-Rafidain University College for Sciences*, *35*(1), 170–185. https://doi.org/10.55562/jrucs.v35i1.268

Semin, Cahyono, B., Muhammad, F., & Barokah, B. (2020). The effect of heating of b20 fuel to combustion characteristic on the diesel engine based on experiment. *International Journal of Marine Engineering Innovation and Research*, *5*(1), 1–9. https://doi.org/10.12962/j25481479.v4i4.5654

Sethin, A., Oo, Y., Thawornprasert, J., & Somnuk, K. (2024). Effects of blended diesel–biodiesel fuel on emissions of a common rail direct injection diesel engine with different exhaust gas recirculation rates. *ACS Omega*, *9*(19), 20906–20918. https://doi.org/10.1021/acsomega.3c10125

Sharma, S., Sharma, S., Singh, M., Singh, P., Singh, R., Maharana, S., Khalilpoor, N., & Issakhov, A. (2021). Computational fluid dynamics analysis of flow patterns, pressure drop, and heat transfer coefficient in staggered and inline shell-tube heat exchangers. *Mathematical Problems in Engineering*, *2021*, 6645128. https://doi.org/10.1155/2021/6645128

Srinivasan, G., Jambulingam, R., Gacem, A., Ahmad, A., Bhutto, J., Yadav, K., Mezni, A., Alharbi, O., Islam, S., Ahn, Y., & Jeon, B. (2022). Effect of fuel preheating on engine characteristics of waste animal fat-oil biodiesel in compression ignition engine. *Polymers*, *14*(18), 3896. https://doi.org/10.3390/polym14183896

Susila, I., Rachimoellah, & Sutantra, I. (2012). The performance of diesel engine using biodiesel fuel from rubber seed oil production by catalytic method. *International Journal of Technology*, *3*(1), 24–34. https://doi.org/10.14716/ijtech.v3i1.79

Tamam, M., Omi, M., Yahya, W., Ithnin, A., Rahman, H., Rahman, M., Kadir, H., Noge, H., Koga, T., Hong, C., Otaka, T., & Kinoshita, E. (2023). Engine performance and emissions evaluation of surfactant-free b30 biodiesel–diesel/water emulsion as alternative fuel. *Scientific Reports*, *13*(1), 10599. https://doi.org/10.1038/s41598-023-37662-4

Titus, K., Ahmed, K., Kumar, S., Santhosh, D., & Geethan, A. (2020). Design and analysis of helical coil heat exchanger. *IOP Conference Series: Materials Science and Engineering*, *923*(1), 012016. https://doi.org/10.1088/1757-899X/923/1/012016

Vijay, V., Aravinda Bhat, K., Shetty, S., & Pai, R. (2016). Design and fabrication of heat exchanger for waste heat recovery from exhaust gas of diesel engine. *Proceedings of the International Conference on Systems, Science, Control, Communication, Engineering and Technology*, *336*(1), 447–455.

Wahile, G., Malwe, P., & Kolhe, A. (2020). Waste heat recovery from exhaust gas of an engine by using a phase change material. *Materials Today: Proceedings*, *28*(4), 2101–2107. https://doi.org/10.1016/j.matpr.2020.03.247

Wu, G., Feng, G., Li, Y., Ling, T., Peng, X., Su, Z., & Zhao, X. (2024). A review of thermal energy management of diesel exhaust after-treatment systems technology and efficiency enhancement approaches. *Energies*, *17*(3), 584. https://doi.org/10.3390/en17030584

Yang, C., & Li, Y. (2021). Fuel-saving performance and main losses of an organic-rankine-cycle-based exhaust heat recovery system in heavy truck application scenarios. *Applied Thermal Engineering*, *193*, 117025. https://doi.org/10.1016/j.applthermaleng.2021.117025

Yilmaz, E., Suzuki, T., Ito, K., Gotama, G., Anggono, W., & Ichiyanagi, M. (2021). Analysis of the spray characteristics of water and water/glycerin mixtures using an interferometric laser imaging for droplet sizing technique. *International Journal of Technology*, *12*(1), 61–70. https://doi.org/10.14716/ijtech.v12i1.4188

Zhang, D., Wu, W., Zhao, L., & Dong, H. (2023). Mathematical investigation of heat transfer characteristics and parameter optimization of integral rolled spiral finned tube bundle heat exchangers. *Processes*, *11*(7), 2192. https://doi.org/10.3390/pr11072192